ADVANCED FUNCTIONAL MATERIALS
www.afm-journal.de

Materials Views
www.MaterialsViews.com

Solution-Processed, Alkali Metal-Salt-Doped, Electron-Transport Layers for High-Performance Phosphorescent Organic Light-Emitting Diodes

*Taeshik Earmme and Samson A. Jenekhe**

High-performance, blue, phosphorescent organic light-emitting diodes (PhOLEDs) are achieved by orthogonal solution-processing of small-molecule electron-transport material doped with an alkali metal salt, including cesium carbonate (Cs_2CO_3) or lithium carbonate (Li_2CO_3). Blue PhOLEDs with solution-processed 4,7-diphenyl-1,10-phenanthroline (BPhen) electron-transport layer (ETL) doped with Cs_2CO_3 show a luminous efficiency (LE) of 35.1 cd A^{-1} with an external quantum efficiency (EQE) of 17.9%, which are two-fold higher efficiency than a BPhen ETL without a dopant. These solution-processed blue PhOLEDs are much superior compared to devices with vacuum-deposited BPhen ETL/alkali metal salt cathode interfacial layer. Blue PhOLEDs with solution-processed 1,3,5-tris(*m*-pyrid-3-yl-phenyl)benzene (TmPyPB) ETL doped with Cs_2CO_3 have a luminous efficiency of 37.7 cd A^{-1} with an EQE of 19.0%, which is the best performance observed to date in all-solution-processed blue PhOLEDs. The results show that a small-molecule ETL doped with alkali metal salt can be realized by solution-processing to enhance overall device performance. The solution-processed metal salt-doped ETLs exhibit a unique rough surface morphology that facilitates enhanced charge-injection and transport in the devices. These results demonstrate that orthogonal solution-processing of metal salt-doped electron-transport materials is a promising strategy for applications in various solution-processed multilayered organic electronic devices.

1. Introduction

Organic light-emitting diodes (OLEDs) are finding various applications in full-color display panels, flexible displays, and solid-state lighting.[1–5] Recently, intensive efforts have been focused on developing phosphorescent OLEDs (PhOLEDs), which utilize triplet excitons to achieve superior performance compare to conventional fluorescent OLEDs.[6–11] Highly efficient multilayered PhOLEDs are generally fabricated by sequential deposition of multilayered structures that facilitate charge-injection and transport from both electrodes to the emission layer (EML). Most high-performance PhOLEDs have been achieved by vacuum-deposition of small molecules involving sequential thermal evaporation to obtain the multilayered structures. In contrast to the intensive efforts made on developing highly efficient multilayered PhOLEDs by thermal vacuum evaporation, reports on solution-processed PhOLEDs are relatively few.[12–16]

Although solution-processing has advantages of low-cost fabrication and/or large-area devices,[17] challenges remain in sequential solution-processing of a multilayered device structure because the solvent used to deposit the subsequent layer can easily dissolve or disrupt the underlayer. One general approach to overcome this problem is to employ orthogonal solvent processing.[18–21] We have reported that many conjugated polymers or dendrimers-based electron-transport materials (ETMs) can be solution-processed from an organic acid solvent onto various underlying polymers, enhancing the performance of polymer OLEDs,[22–26] polymer transistors,[18] or polymer solar cells.[27,28] More recently, we have shown that high performance solution-processed multilayered PhOLEDs can be realized by orthogonal solution-processing of new oligoquinoline ETMs[29,30] and other commercially available small molecule ETMs.[31]

Despite the demonstration of multilayered device structures fabricated by orthogonal solution-processing, improving electron-injection and transport from the metal cathode is a major challenge in realization of all-solution-processed PhOLEDs with higher performance. Because widely used metal cathodes (e.g., Al, Ag) have a high work function (≈4.2 eV) which leads to high electron-injection barriers between the ETM and the cathode, cathode interfacial materials such as alkali metal halides (e.g. LiF, CsF) or low work function metals (e.g., Ca, Ba, or Mg) are generally inserted as a thin interlayer (≈0.5 to 2 nm) between the ETM and cathode to achieve facile electron injection. Another approach to improve electron-injection/transport is by doping the ETM with organic,[32–34] inorganic,[35] or low-work-function metal[36] n-type dopants to modify the interface electronic structure and/or to enhance bulk conductivity of the ETMs.

Various n-type doping approaches and basic mechanisms have been proposed and studied to achieve an increased charge carrier concentration with high conductivity to realize

T. Earmme, Prof. S. A. Jenekhe
University of Washington
Department of Chemical Engineering
and Department of Chemistry
Benson Hall, Box 351750, Seattle, WA 98195-1750, USA
E-mail: jenekhe@u.washington.edu

DOI: 10.1002/adfm.201201366

high-performance OLEDs. N-type doping of the organic ETMs is known to be challenging due to the difficulty of finding suitable n-type dopants. For efficient doping, the HOMO level of n-type dopant must be higher than the LUMO level of the organic semiconductors, which is generally unstable in the air.[37] The use of alkali metal is well-known approach to improve electron-injection from cathode. For example, an evaporation of Li metal or LiF monolayer or co-evaporation of the dopants into bulk organic ETMs have been known as an efficient n-type doping method.[38–41] The influence of n-doping by Li metal or LiF on tris(8-hydroxyquinoline)aluminum (Alq_3) ETM has been studied in detail by X-ray photoelectron spectroscopy (XPS) or ultraviolet photoemission spectroscopy (UPS) indicating a chemical reaction of LiF and Al which may release Li ions into the bulk organic ETM.[40,41]

There also have been many efforts on utilizing organic materials with a high-lying HOMO as n-type dopants which would act as strong electron donor to organic ETMs. The use of strong reducing molecule such as cobaltocene ($CoCp_2$) was reported and investigated, showing that the Fermi level shifted toward the unoccupied states of the host ETM, which resulted in three orders of magnitude current increase.[42] Other examples of n-type dopants include electrochemically reduced form of the transition metal complex[43] or salts of cationic dyes as strong molecular donors.[44,45]

Recently, alkali metal salts have proven to be effective n-type dopant to enhance electron-injection and transport of organic ETMs. For example, cesium carbonate (Cs_2CO_3),[46–49] lithium carbonate (Li_2CO_3),[50] cesium fluoride (CsF),[51] and lithium fluoride (LiF)[52] have been co-evaporated as n-type dopants with various organic ETMs. The n-type doping effect of alkali metal salt was demonstrated by surface analysis techniques showing that the Fermi level of the organic ETMs shifts toward the LUMO edge.[35] The proposed mechanism of n-type doping effect was that the alkali metal salt such as Cs_2CO_3 would decompose into a mixture of Cs and oxides of Cs during thermal evaporation, which may have sufficient n-doping ability.[48,49]

Nevertheless, such a doping is mainly carried out by thermal evaporation or co-evaporation under high vacuum especially in the case of alkali metal salts. Furthermore, for the co-evaporation process, a precise control of the co-deposition rate via complicated vacuum thermal evaporation process is critical to obtain exact dopant to host ratio and this is highly challenging and economically undesirable.

In this paper, we report for the first time that organic small-molecule electron-transport materials can be doped with alkali metal salts by solution-processing of the electron transport layer (ETL) to achieve high-performance all-solution-processed PhOLEDs. We found that incorporation of the dopant into the ETL by solution-processing significantly changes the surface morphology of ETL forming a good interfacial contact between ETL and metal cathode, leading to facile electron-injection and transport. Our results suggest that solution-processing of metal salt doped small-molecule ETMs is a new strategy that could enable the fabrication of various high-performance multilayered all-solution-processed organic electronic devices. High performance solution-processed blue PhOLEDs were achieved by sequential solution-processing of electron-transport material doped with an alkali metal salt, cesium carbonate (Cs_2CO_3) or lithium carbonate (Li_2CO_3). PhOLEDs based on FIrpic blue triplet emitter-doped poly(*N*-vinylcarbazole) emission layer and a solution-processed 4,7-diphenyl-1,10-phenanthroline (Bathophenanthroline, BPhen)[53–55] electron-transport layer (ETL) doped with Cs_2CO_3 show a luminous efficiency (LE) of 35.1 cd A^{-1} at a brightness of 1820 cd m^{-2} with a power efficiency of 15.0 lm W^{-1} and an external quantum efficiency of 17.9%. Furthermore, our approach of solution-processing of alkali metal salt doped ETL was readily extended to other small-molecule electron-transport materials, including 1,3,5-tris(4-pyridinquinolin-2-yl)benzene (TPyQB),[30] 1,3,5-tris(*m*-pyrid-3-yl-phenyl)benzene (TmPyPB),[56,57] and 1,3-bis(3,5-di(pyridine-3-yl) phenyl)benzene (BmPyPB) (**Scheme 1**).[58] The blue PhOLEDs with solution-processed TmPyPB ETL doped with Cs_2CO_3 show a high LE value of 37.7 cd A^{-1} at a brightness of 1300 cd m^{-2} with a power efficiency of 14.1 lm W^{-1} and an external quantum efficiency of 19.0%, which is the highest performance reported to date for all-solution-processed blue PhOLEDs.

2. Results and Discussion

2.1. Performance of PhOLEDs with Alkali Metal Salt Doped BPhen ETLs

We fabricated solution-processed multilayered PhOLEDs with polymer-based blue phosphorescent emission layer (EML) and solution-deposited BPhen electron-transport layer (ETL) doped with an alkali metal salt (M_2CO_3, M = Li, Cs) dopant, Cs_2CO_3 or Li_2CO_3. The concentration of the dopant in the ETL was: 2.5, 5.0, 7.5, 10.0, 12.5 or 15.0 wt% Cs_2CO_3 and 1.0, 2.5, 5.0, 7.5 or 10.0 wt% Li_2CO_3. The blend of BPhen and alkali metal salt, BPhen:Cs_2CO_3 or BPhen:Li_2CO_3 ETL, was deposited from a formic acid (FA)/water (H_2O) solvent mixture (FA:H_2O = 3:1)

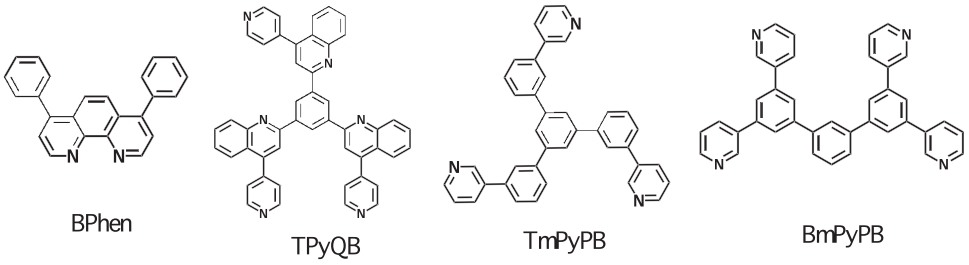

Scheme 1. Molecular structures of electron-transport materials.

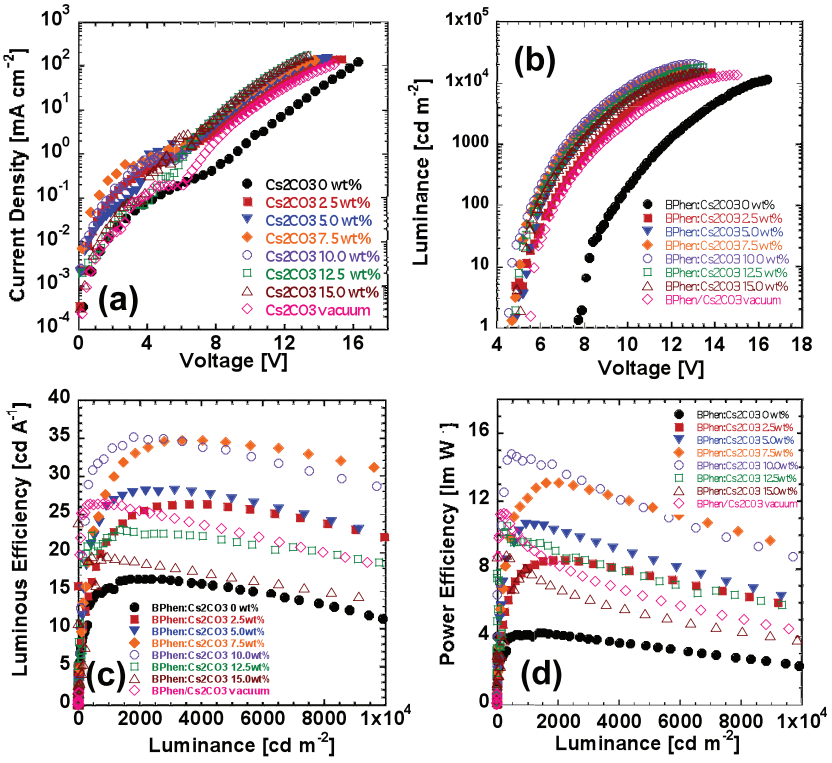

Figure 1. Blue PhOLEDs with BPhen ETL doped with Cs_2CO_3: a) Current density (*J*)–voltage (*V*); b) luminance (*L*)–voltage (*V*); c) luminous efficiency (*LE*)–luminance (*L*); and d) power efficiency (*PE*)–luminance (*L*) curves. Device structures: ITO/PEDOT:PSS(30 nm)/EML(70 nm)/solution-processed BPhen:Cs_2CO_3 ETL(20 nm)/Al (100 nm), ETL doped with different concentration of Cs_2CO_3; and ITO/PEDOT:PSS(30 nm)/EML(70 nm)/vacuum-deposited BPhen ETL(20 nm)/vacuum-deposited Cs_2CO_3(1 nm)/Al (100 nm).

onto the EML.[29,30] A series of PhOLEDs with solution-processed BPhen:M_2CO_3 ETL were fabricated: ITO/PEDOT:PSS/EML/BPhen:M_2CO_3/Al; the metal salt (M_2CO_3, M = Cs, Li) concentration was varied in the ETL. To verify the relative effectiveness of the solution-processed BPhen:M_2CO_3-doped ETLs, PhOLEDs with a vacuum-deposited BPhen ETL and an alkali metal salt electron-injection layer (EIL) were also fabricated: ITO/PEDOT:PSS/EML/vacuum-deposited BPhen/vacuum-deposited Cs_2CO_3 or Li_2CO_3/Al. The detailed PhOLED fabrication procedures are described in the Experimental Section.

Figure 1 shows the performance of PhOLEDs with solution-processed BPhen:Cs_2CO_3 ETL. As shown in Figure 1a–d (Figure S1a, Supporting Information), the PhOLEDs with solution-deposited BPhen ETL without Cs_2CO_3 dopant (BPhen: Cs_2CO_3 0 wt%) showed a high turn-on voltage of 7.7 V, a drive voltage of 16.4 V and lower current density compared to other devices with BPhen ETL doped with Cs_2CO_3. The higher current density values of the PhOLEDs with doped BPhen ETL at low voltages imply that charge injection from cathode has been improved by increased conductivity of the doped ETL. The performance of the PhOLEDs dramatically changes when Cs_2CO_3 is incorporated into BPhen ETL (Figure 1, **Table 1**). PhOLEDs with 2.5 wt%

Table 1. Device chracteristics of solution-processesd PhOLEDs with BPhen ETL doped with Cs_2CO_3.[a)]

ETL[b)]	Dopant concentration [wt%]	V_{on}[d)] [V]	Drive voltage [V]	Current density [mA cm^{-2}]	Luminance [cd m^{-2}]	Device efficiency [cd A^{-1}, lm W^{-1}, (%EQE)]
BPhen	0.0	7.7	16.4	133.4	11200	8.4, 1.6, (4.3)
			12.6	*11.5*	*1890*	*16.5, 4.1, (8.4)*
BPhen:	2.5	4.8	13.9	108.9	14800	13.6, 3.0, (6.9)
Cs_2CO_3			*10.2*	*13.6*	*3600*	*26.4, 8.5, (13.5)*
BPhen:	5.0	4.8	13.2	107.5	14600	13.6, 3.2, (6.9)
Cs_2CO_3			*8.9*	*9.0*	*2530*	*28.1, 10.5, (14.3)*
BPhen:	7.5	4.6	12.8	103.3	18200	17.6, 4.3, (8.9)
Cs_2CO_3			*8.7*	*10.2*	*3520*	*34.7, 13.1, (17.7)*
BPhen:	10.0	4.5	12.6	144.3	20100	13.9, 3.4, (7.0)
Cs_2CO_3			*7.8*	*5.2*	*1820*	*35.1, 15.0, (17.9)*
BPhen:	12.5	4.8	12.4	177.5	17700	9.6, 2.5, (4.9)
Cs_2CO_3			*7.5*	*6.0*	*1360*	*22.9, 9.6, (11.7)*
BPhen:	15.0	4.9	13.6	187.8	15100	8.0, 1.9, (4.0)
Cs_2CO_3			*7.6*	*4.2*	*830*	*19.6, 8.1, (10.0)*
BPhen/	–	5.5	15.1	112.6	13400	11.9, 2.5, (6.1)
Cs_2CO_3 [c]			*7.6*	*1.2*	*320*	*26.9, 11.7, (13.7)*

[a)]Values in italics correspond to those at maximum device efficiencies; [b)]PhOLEDs with solution-deposited BPhen ETL doped with Cs_2CO_3 or with vacuum-deposited BPhen/Cs_2CO_3 ETL/EIL. Device structures: ITO/PEDOT:PSS/EML/ETL/Al with solution-deposited doped BPhen ETL; and [c)]ITO/PEDOT:PSS/EML/BPhen/Cs_2CO_3/Al with vacuum-deposited BPhen and Cs_2CO_3; [d)]Turn-on voltage (at brightness of 1 cd m^{-2}).

Cs_2CO_3 dopant showed a significantly reduced turn-on voltage (4.8 V), drive voltage (13.9 V), and also a significantly increased luminous efficiency (LE) of 26.4 cd A^{-1} with a power efficiency (PE) of 8.5 lm W^{-1} (external quantum efficiency (EQE) = 13.5%). This represents a 1.6-fold higher efficiency compared to the device without Cs_2CO_3 dopant. As the concentration of Cs_2CO_3 in BPhen ETL increased from 2.5 to 10.0 wt%, the PhOLEDs showed much enhanced performance; the current density and maximum luminance (brightness) increased while the turn-on voltage and drive voltage decreased (Figure 1a,b, Table 1). The blue PhOLEDs with solution-processed BPhen:Cs_2CO_3 (10.0 wt% Cs_2CO_3) showed the highest luminous efficiency (LE) of 35.1 cd A^{-1} (at 1820 cd m^{-2}) (Figure 1c) and the maximum power efficiency (PE) of 15.0 lm W^{-1} (Figure 1d) with an EQE of 17.9%, which is more than two-fold superior compared to the devices without Cs_2CO_3 doping. Even compared to the devices with vacuum-deposited BPhen ETL and Cs_2CO_3 EIL layers, PhOLEDs with solution-processed BPhen ETL doped with Cs_2CO_3 showed much superior performance. We note that PhOLEDs with solution-processed ETL reached the maximum efficiency at high brightness (1820–3600 cd m^{-2}) while the devices with vacuum-deposited ETL/EIL showed the maximum efficiency at low brightness of 320 cd m^{-2}. Furthermore, PhOLEDs with vacuum-deposited ETL/EIL showed much more severe efficiency roll-off (Figure 1c,d) compared to the devices with solution-processed doped ETLs. These results suggest that the solution-processing of metal salt doped small-molecule electron-transport layer is promising for achieving high efficiency devices with high brightness.

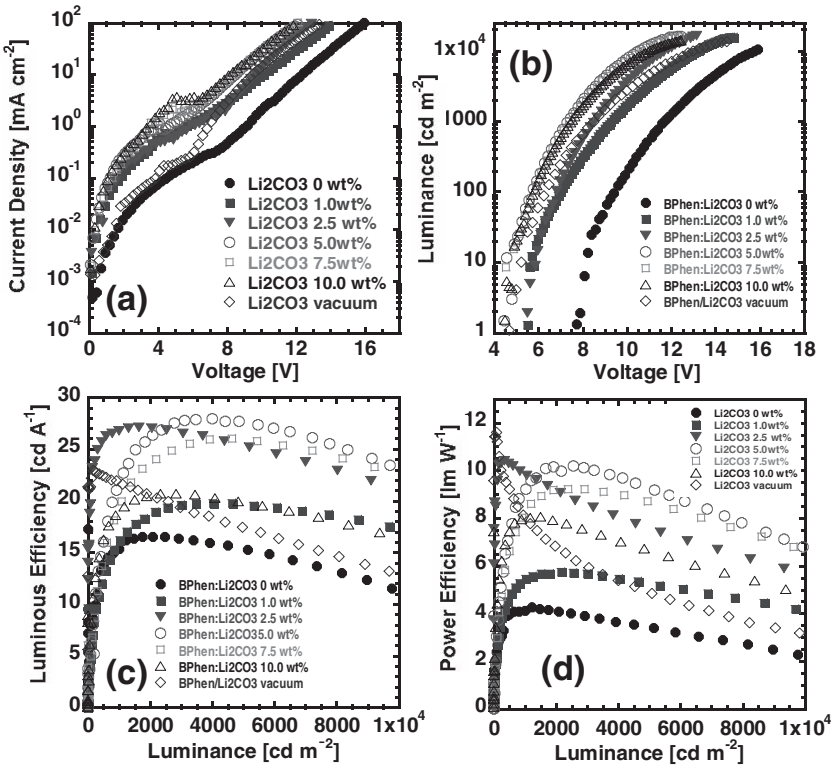

Figure 2. Blue PhOLEDs with BPhen ETL doped with Li_2CO_3: a) current density (*J*)–voltage (*V*); b) luminance (*L*)–voltage (*V*); c) luminous efficiency (*LE*)–luminance (*L*); and d) power efficiency (*PE*)–luminance (*L*) curves. Device structures: ITO/PEDOT:PSS(30 nm)/EML(70 nm)/solution-processed BPhen:Li_2CO_3 ETL(20 nm)/Al (100 nm), BPhen ETL doped with different concentration of Li_2CO_3; and ITO/PEDOT:PSS(30 nm)/EML(70 nm)/vacuum-deposited BPhen ETL(20 nm)/vacuum-deposited Li_2CO_3(1 nm)/Al (100 nm).

A further increase of the Cs_2CO_3 concentration in BPhen:Cs_2CO_3 ETL to 12.5 and 15.0 wt% resulted in decreased device performance, even though these later PhOLEDs have similar current density (*J*–*V*) characteristics as the devices with 10.0 wt% Cs_2CO_3 (Figure 1a). PhOLEDs with 12.5 and 15.0 wt% Cs_2CO_3–doped ETLs showed a higher turn-on and drive voltages and lower device efficiencies compared to the devices with 10.0 wt% Cs_2CO_3 (Figure 1b–d, Table 1). These later PhOLEDs (> 10% Cs_2CO_3 ETLs) also showed severe efficiency roll-off as the brightness increases, similar to the devices with vacuum-deposited ETL/EIL. The optimum doping concentration in BPhen:Cs_2CO_3 ETLs is thus 10.0 wt% Cs_2CO_3.

The *J*–*V*, *L*–*V*, *LE*–*L*, and the *PE*–*L* characteristics of PhOLEDs with BPhen ETLs doped with Li_2CO_3 are shown in **Figure 2**a–d (Figure S1b, Supporting Information). Incorporation of Li_2CO_3 in the solution-processed BPhen ETL show significantly improved device performance. PhOLED with 1.0 wt% of Li_2CO_3 showed an increased LE value of 19.8 cd A^{-1} (at 4030 cd m^{-2}) and a PE value of 5.7 lm W^{-1} (EQE of 10.1%) compared to the device without Li_2CO_3 doping. As the Li_2CO_3 concentration increased to 2.5 and 5.0 wt%, the PhOLEDs showed much more enhanced performance. PhOLEDs with solution-deposited BPhen ETL doped with 2.5 wt% Li_2CO_3 gave a LE value of 27.1 cd A^{-1} and a PE value of 10.4 lm W^{-1} (EQE of 13.8%), while the PhOLEDs with 5.0 wt% Li_2CO_3 showed the highest device performance with an LE value of 27.9 cd A^{-1} and EQE of 14.2% (PE = 10.1 lm W^{-1}) with significantly reduced turn-on voltage of 4.4 V and a drive voltage of 12.3 V compared to the devices without Li_2CO_3 dopant (Figure 2c,d, **Table 2**). However, a further increase of the Li_2CO_3 concentration to 7.5 and 10.0 wt% resulted in a decreased device performance with LE values of 26.0 and 20.7 cd A^{-1} (PE values of 9.2 and 8.0 lm W^{-1}), respectively, even though the *J*–*V* characteristics of these later devices were similar compared to the devices with 5.0 wt% Li_2CO_3-doped ETL (Figure 2a).

Similar to the PhOLEDs with BPhen:Cs_2CO_3 ETLs, PhOLEDs with solution-processed BPhen ETL doped with 2.5–5.0 wt% Li_2CO_3 had superior performances compare to the devices with vacuum-deposited BPhen ETL/Li_2CO_3 EIL. We also note that PhOLEDs with vacuum-deposited ETL/EIL showed the maximum LE value (23.0 cd A^{-1}) and PE value (11.8 lm W^{-1}) at low brightness (≈120 cd m^{-2}), whereas the devices with solution-processed ETL doped with Li_2CO_3 showed the highest efficiency at high brightness (1720–4340 cd m^{-2}). These results clearly demonstrate that the solution-processing of ETL doped

Table 2. Device chracteristics of solution-processed PhOLEDs with BPhen ETL doped with Li_2CO_3.[a)]

ETL[b)]	Dopant concentration [wt%]	V_{on}[d)] [V]	Drive voltage [V]	Current density [mA cm^{-2}]	Luminance [cd m^{-2}]	Device efficiency [cd A^{-1}, lm W^{-1}, (%EQE)]
BPhen	0.0	7.7	16.4	133.4	11200	8.4, 1.6, (4.3)
			12.6	*11.5*	*1890*	*16.5, 4.1, (8.4)*
BPhen:	1.0	5.5	14.8	148.4	15700	10.6, 2.5, (5.4)
Li_2CO_3			*11.4*	*20.4*	*4030*	*19.8, 5.7, (10.1)*
BPhen:	2.5	5.4	13.8	162.9	17800	11.0, 2.5, (5.6)
Li_2CO_3			*9.1*	*6.4*	*1720*	*27.1, 10.4, (13.8)*
BPhen:	5.0	4.4	12.3	100.8	14500	14.5, 3.7, (7.4)
Li_2CO_3			*8.9*	*12.8*	*3600*	*27.9, 10.1, (14.2)*
BPhen:	7.5	4.5	12.5	120.0	15600	13.0, 3.3, (6.6)
Li_2CO_3			*9.2*	*16.7*	*4340*	*26.0, 9.2, (13.2)*
BPhen:	10.0	4.6	12.5	162.2	15800	9.8, 2.5, (5.0)
Li_2CO_3			*8.4*	*11.7*	*2430*	*20.7, 8.0, (10.6)*
BPhen/	–	4.6	14.7	163.9	13400	8.1, 1.7, (4.1)
Li_2CO_3[c)]			*6.5*	*0.52*	*120*	*23.0, 11.7, (11.7)*

[a)]Values in italics correspond to those at maximum device efficiencies; [b)]PhOLEDs with solution-deposited BPhen ETL doped with Li_2CO_3 or with vacuum-deposited BPhen/Li_2CO_3 ETL. Device structures: ITO/PEDOT:PSS/EML/ETL/Al with solution-deposited doped BPhen ETL; and [c)]ITO/PEDOT:PSS/EML/BPhen/Li_2CO_3/Al with vacuum-deposited BPhen and Li_2CO_3; [d)]Turn-on voltage (at brightness of 1 cd m^{-2}).

with alkali metal salt is a promising strategy to achieve high-performance blue PhOLEDs with high brightness. The device characteristics of the blue PhOLEDs with solution-processed BPhen ETL are summarized in Table 1 and 2.

The electroluminescence (EL) spectra of all the blue PhOLEDs, including those containing BPhen:Cs_2CO_3 or BPhen:Li_2CO_3 ETLs, are identical in lineshape with a maximum peak at 472 nm, which originates from the FIrpic blue triplet emitter (**Figure 3**).[26,27] The Commission Internationale de L'Eclairage (CIE) 1931 coordinates of the devices were identical at (0.14, 0.28). We observed a slight increase of the vibronic shoulder around 500 nm in the case of PhOLEDs with solution-processed BPhen ETLs doped with 7.5 wt% Cs_2CO_3 and 5.0 wt% Li_2CO_3, which can be due to microcavity effects.[38]

2.2. PhOLEDs with Various Small-Molecule ETMs Doped with Cs_2CO_3

To test how general our approach of solution-processing of alkali metal salt doped electron transport materials is, we investigated various other known electron transport materials, including 1,3,5-tris(4-pyridinquinolin-2-yl)benzene (TPyQB),[30] 1,3,5-tris(*m*-pyrid-3-yl-phenyl)benzene (TmPyPB),[56,57] and 1,3-bis(3,5-di(pyridine-3-yl)phenyl)benzene (BmPyPB).[58] The solution-processed ETL was doped with 5.0, 7.5, or 12.5 wt% Cs_2CO_3 and incorporated into multilayered blue PhOLEDs similar to BPhen:Cs_2CO_3 ETL devices described above.

We initially fabricated PhOLEDs using solution-processed TPyQB ETL doped with Cs_2CO_3. (Figure S2, Supporting Information). PhOLEDs with solution-processed TPyQB ETL without Cs_2CO_3 doping showed a turn-on voltage of 5.5 V, a drive voltage

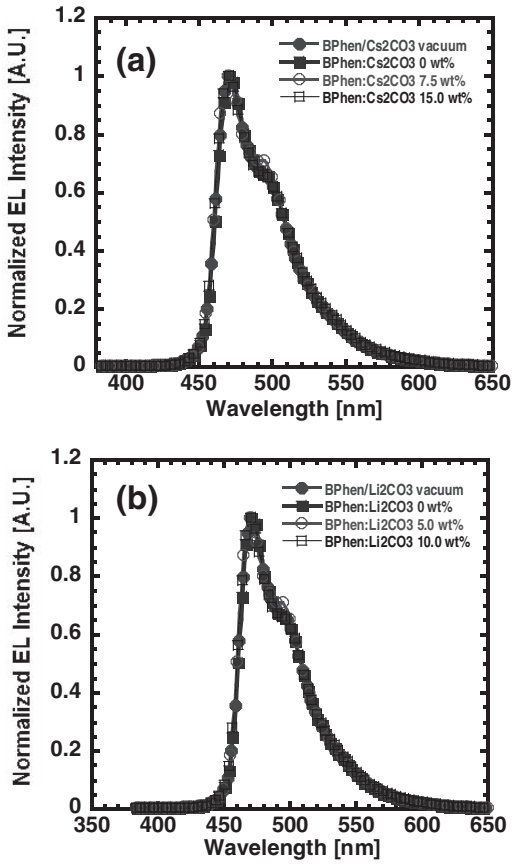

Figure 3. Normalized EL spectra of blue PhOLEDs with: a) BPhen:Cs_2CO_3 and b) BPhen:Li_2CO_3 ETLs at the maximum brightness.

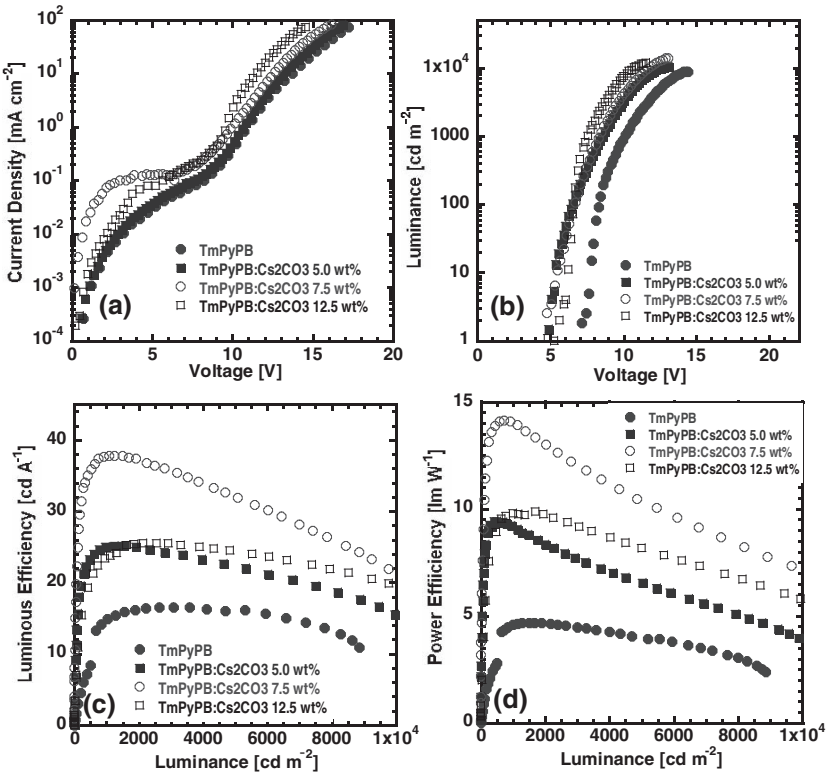

Figure 4. Blue PhOLEDs with TmPyPB ETL doped with Cs_2CO_3: a) Current density (*J*)–voltage (*V*); b) luminance (*L*)–voltage (*V*); c) luminous efficiency (*LE*)–luminance (*L*); and d) power efficiency (*PE*)–luminance (*L*) curves. Device structures: ITO/PEDOT:PSS(30 nm)/EML(70 nm)/solution-processed TmPyPB:Cs_2CO_3 ETL(20 nm)/Al (100 nm), TmPyPB ETL doped with different concentration of Cs_2CO_3.

of 13.7 V and a lower current density compared to devices with TPyQB ETL doped with Cs_2CO_3. The performance of the PhOLEDs increased dramatically after incorporating Cs_2CO_3 into the TPyQB ETL. PhOLEDs with 7.5 wt% Cs_2CO_3-doped TPyQB ETL showed the highest performance with a reduced turn-on voltage (4.4 V), drive voltage (12.8 V), and a significantly increased LE value of 33.6 cd A^{-1} with a PE value of 8.2 lm W^{-1} (EQE = 17.1%). Clearly, PhOLEDs with Cs_2CO_3-doped TPyQB ETL have far superior performance than those without Cs_2CO_3 doping. (Figure S2c,d, Supporting Information).

Electron-transport materials with pyridyl groups were reported by Kido and co-workers[44,45] as high triplet energy ETMs. For example, TmPyPB was reported to have a high triplet energy of 2.78 eV and a high electron mobility of $\mu_e = 1.0 \times 10^{-3}$ cm^2 V^{-1}s^{-1}. As shown in **Figure 4**, the PhOLEDs with undoped TmPyPB had a much lower performance (LE = 16.5 cd A^{-1}, PE = 4.7 lm W^{-1}, and EQE = 8.4%), whereas Cs_2CO_3-doped TmPyPB ETL led to a large enhancement of device performance. The performance of PhOLEDs with TmPyPB:Cs_2CO_3 (7.5 wt%) ETL showed a LE value of 37.7 cd A^{-1} (PE = 14.1 lm W^{-1}, EQE = 19.0%), which is the highest performance reported to date for all-solution-processed blue PhOLEDs. We also fabricated PhOLEDs with solution-processed BmPyPB:Cs_2CO_3 ETLs and, as expected, the PhOLEDs with BmPyPB ETL doped with Cs_2CO_3 similarly had a large enhancement in performance compared to non-doped ETL devices. The devices with BmPyPB ETL doped with 7.5 wt% Cs_2CO_3 showed an LE value of 37.4 cd A^{-1} at a high brightness of 1760 cd m^{-2}, and a PE value of 16.1 lm W^{-1} (Figure S3, Supporting Information). The performance of blue PhOLEDs incorporating BmPyPB:Cs_2CO_3 ETL at the optimum doping concentration of 7.5 wt% Cs_2CO_3 is essentially identical with that of devices incorporating TmPyPB:Cs_2CO_3 at the same doping concentration. Further increase of the Cs_2CO_3 concentration in the TmPyPB:Cs_2CO_3 and BmPyPB:Cs_2CO_3 ETLs resulted in decreased performance of the PhOLEDs (Figure 4 and Figure S3, Supporting Information) and these trends are very similar to those of PhOLEDs incorporating BPhen:Cs_2CO_3 ETLs.

These results demonstrate that the solution-processing of ETL doped with alkali metal salt is applicable to various small-molecule electron-transport materials[31] of current interest for the fabrication of all-solution-processed multilayered OLEDs and other organic electronic devices. Among the four electron-transport materials investigated, blue PhOLEDs with solution-processed TmPyPB:Cs_2CO_3 ETLs and BmPyPB:Cs_2CO_3 ETLs have the best performance and thus TmPyPB and BmPyPB are superior to BPhen and TPyQB in this respect. We can also conclude that Cs_2CO_3 is superior to Li_2CO_3 as an alkali metal salt dopant of the series of small-molecule electron-transport materials.

2.3. Surface Morphology of Doped BPhen ETLs

The surface morphology of solution-deposited alkali metal salt-doped ETLs was investigated by atomic force microscopy (AFM). **Figure 5** shows AFM topographical height and the corresponding phase images of solution-deposited BPhen ETLs with different concentrations of Cs_2CO_3. BPhen ETL without Cs_2CO_3 doping has a smooth surface with root-mean-square (RMS) roughness of 0.312 nm (Figure 5a) whereas the solution-deposited Cs_2CO_3-doped BPhen ETLs show a significant change in surface morphology as the Cs_2CO_3 concentration increases (Figure 5b–f). BPhen ETLs with 5.0 and 7.5 wt% Cs_2CO_3 have rougher surfaces (RMS values = 0.570 and 0.840 nm) compared to the BPhen ETL without Cs_2CO_3 doping (Figure 5b,c). As the Cs_2CO_3 concentration increases to 10.0 wt%, the ETL surface morphology becomes even much rougher, having an RMS roughness value of 1.12 nm (Figure 5d). In the light of the surface morphology variation with Cs_2CO_3 concentration in the ETL, we suggest that in addition to n-doping effects of the alkali metal salt, the surface roughness of the solution-processed ETL, which enhances the ETL/Al contact area and thus facilitates efficient electron-injection. According to our previous reports, the rough surface morphology and vertical nanopillars formed in the solution-processed ETL leads to enhanced charge transport in the vertical

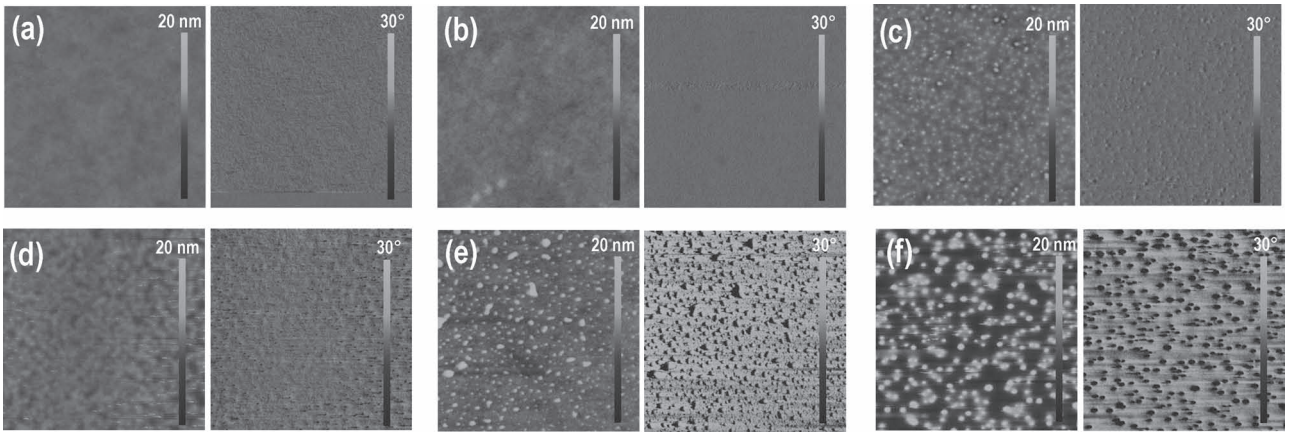

Figure 5. AFM topographical height images (left, 5 μm × 5 μm) and the corresponding phase images (right, 5 μm × 5 μm) of solution-processed BPhen ETL films doped with different concentration of Cs_2CO_3: a) 0 wt%; b) 5.0 wt%; c) 7.5 wt%; d) 10.0 wt%; e) 12.5 wt%; and f) 15.0 wt%.

direction and also provide good contact between ETL and Al cathode for facile electron-injection.[29–31]

On the other hand, BPhen ETLs with a high Cs_2CO_3 concentration of 12.5 and 15.0 wt% have extremely rough surfaces with RMS roughness values of 2.53 and 5.53 nm (Figure 5e,f). At these high concentrations a clear phase separation in the BPhen:Cs_2CO_3 blend appears to occur and explains the observed decrease in device performance at high (>10.0 wt%) Cs_2CO_3 concentrations. A significantly decreased charge-injection from cathode and charge-transport in the ETL can be expected when a separate insulating Cs_2CO_3 phase emerges in the ETL.

A similar trend was observed in the solution-processed BPhen ETLs doped with Li_2CO_3. A smooth surface was observed in the AFM images of the solution-deposited BPhen ETL without the dopant (RMS value = 0.312 nm, **Figure 6**a) and the BPhen ETL doped with 1.0 wt% Li_2CO_3 (RMS value = 0.331 nm, Figure 6b), whereas BPhen ETLs doped with 2.5 (Figure 6c) and 5.0 wt% (Figure 6d) showed increased surface roughness with RMS values of 0.477 and 0.581 nm, respectively. The increased surface roughness is consistent with the improved performance of PhOLEDs with ETLs at these doping levels. However, solution-processed BPhen ETL at a higher concentration (10.0 wt% Li_2CO_3) showed severe phase-separated surface morphology (Figure 6f). We can also understand the decreased performance of devices with BPhen ETLs doped at 10.0 wt% Li_2CO_3 as a consequence of such a phase-separated surface morphology. The observed surface morphology variation with alkali metal salt concentration in the doped ETL correlates very well with a similar observed variation of device performance with concentration of the alkali metal salt.

2.4. Electron- and Hole-Dominant Devices

To further investigate the charge-injection and transport properties in PhOLEDs containing solution-processed ETL doped with alkali metal salts (M_2CO_3, M = Cs, Li), two types of single-carrier dominant devices were fabricated, including electron-dominant devices, ITO/polymer host (70 nm)/solution-deposited BPhen:M_2CO_3 ETL (20nm)/Al, and hole-dominant devices, ITO/PEDOT:PSS (30 nm)/polymer host (70 nm)/

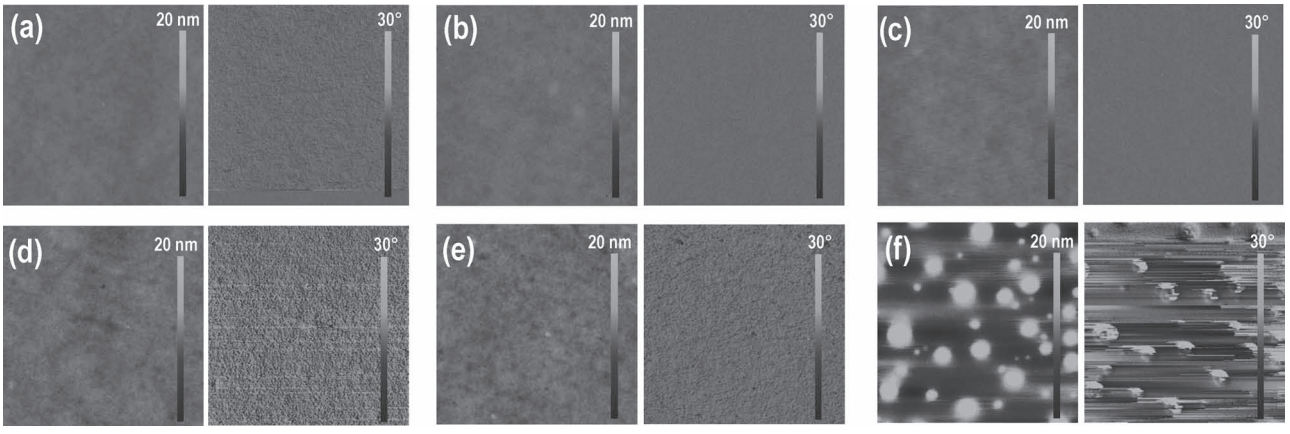

Figure 6. AFM topographical height images (left, 5 μm × 5 μm) and the corresponding phase images (right, 5 μm × 5 μm) of solution-processed BPhen ETL films doped with different concentration of Li_2CO_3: a) 0 wt%; b) 1.0 wt%; c) 2.5 wt%; d) 5.0 wt%; e) 7.5 wt%; and f) 10.0 wt%.

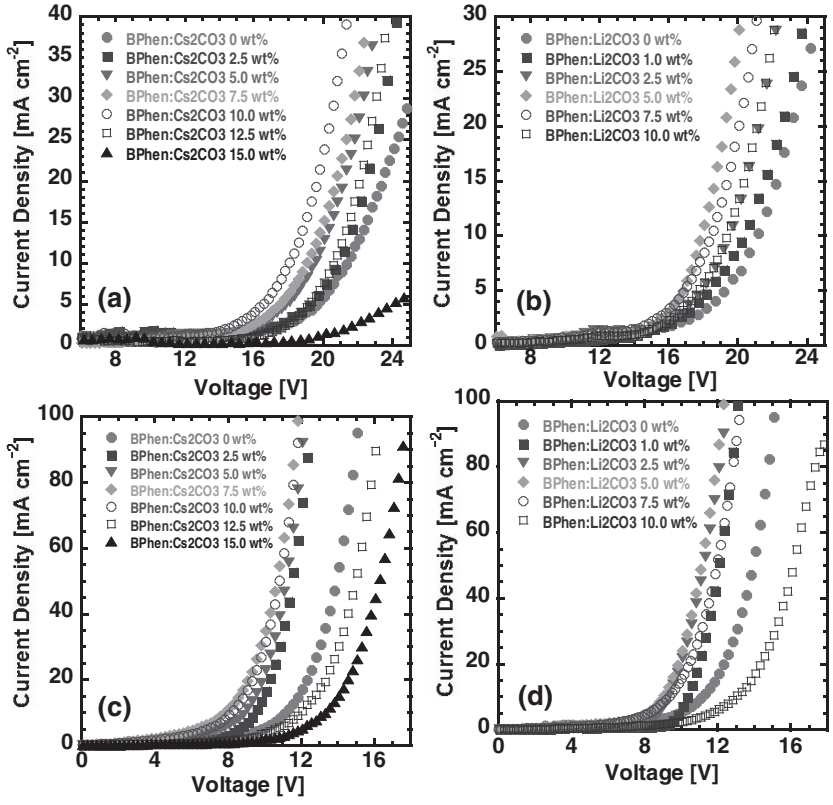

Figure 7. Single charge-carrier dominant devices: a) electron-dominant devices with solution-processed BPhen:Cs_2CO_3 ETLs; b) electron-dominant devices with solution-processed BPhen:Li_2CO_3 ETLs; c) hole-dominant devices with solution-processed BPhen:Cs_2CO_3 ETLs; and d) hole-dominant devices with solution-processed BPhen:Li_2CO_3 ETLs. Device structures of electron-dominant devices: ITO/polymer host(70 nm)/solution-processed BPhen:Cs_2CO_3 ETL (20 nm)/Al; and hole-dominant devices: ITO/PEDOT:PSS(30 nm)/polymer host(70 nm)/ solution-processed BPhen:Li_2CO_3 ETL (20 nm)/Au.

solution-deposited BPhen:M_2CO_3 ETL (20 nm)/Au. The polymer host consisted of PVK and OXD-7 with the same ratio of 6:4 as in the PhOLEDs, except that the blue triplet emitter FIrpic was excluded. It is assumed that hole-injection from the ITO can be suppressed by the large energy barrier between the work function of ITO ($\Phi_f \approx 4.5$ eV) and the ionization potential (IP) values of the polymer host (5.8 eV for PVK and 6.2 eV for OXD-7) in the electron-dominant devices. Similarly, electron-injection can be prevented by the energy barrier between the work function of Au ($\Phi_f = 5.0$ eV) and the electron affinity (EA) of BPhen (3.0 eV) in the hole-dominant devices.

Figure 7 shows the single charge carrier-dominant devices with solution-processed BPhen:M_2CO_3 ETL with varying concentration of the M_2CO_3 dopants (M = Cs, Li). The *J–V* characteristics of the electron-dominant devices with solution-processed BPhen ETL doped with Cs_2CO_3 and Li_2CO_3 are shown in Figure 7a and 7b, respectively. A significant increase of the current density was observed when the BPhen ETL was doped by the alkali metal salt in electron-dominant devices. As shown by the highest current densities, the electron-injection and transport was the most efficient when the Cs_2CO_3 and Li_2CO_3 doping concentrations were 10.0 wt% and 5.0 wt%, respectively. This trend matches well with the observed highest performance of PhOLEDs with BPhen doped with alkali metal salt. These results imply that electron-injection and transport are enhanced by incorporating alkali metal salt into the ETL, achieving the maximum current density at optimum concentration of the alkali metal salt. However, further increase of the M_2CO_3 dopant concentration (12.5 and 15.0 wt% for Cs_2CO_3, 7.5 and 10.0 wt% for Li_2CO_3) results in decrease of the current density. The trend also matches with the observed decrease PhOLED performance at the higher doping levels, presumably due to the phase separation in the solution-processed BPhen:M_2CO_3 blend ETLs which interrupts facile electron-injection and transport.

The *J–V* characteristics of the hole-dominant devices containing the solution-processed BPhen ETL doped with Cs_2CO_3 and Li_2CO_3 are shown in Figure 7c and 7d, respectively. The trends are similar to those for electron-dominant devices in that increased current density is seen with incorporation of alkali metal salt doped ETL. It has been reported that devices with BPhen ETL doped with Li_2CO_3 by vacuum co-deposition showed reduced hole-current as the dopant concentration increased.[50] In contrast, the solution-processed BPhen ETL doped with alkali metal salt show enhanced hole-current and this can be understood to result from a good contact between the ETL and Au electrode enabled by solution-processing. This result implies that the strategy applied to improve charge-injection and transport by tuning the surface morphology of the ETMs to improve the interfacial contact between the ETL and metal cathode is not limited to Al, but can also be applied to other metal electrodes. However, the current density of the hole-dominant devices is severely reduced at higher concentrations of the dopant (Cs_2CO_3 = 12.5 – 15.0 wt%, Li_2CO_3 = 10.0 wt%), presumably due to the reduced charge-injection and transport when phase separation occurs in the BPhen:M_2CO_3 blend ETL. This means that for a given electron-transport material there is an optimum alkali metal salt doping level for maximum PhOLED performance.

2.5. Space-Charge-Limited Current (SCLC) Measurement of Solution-Processed BPhen ETLs

We investigated the electron transport properties of the solution-processed alkali metal salt doped BPhen ETL films by space-charge-limited current (SCLC) measurement. The current-voltage (*I–V*) characteristics of the SCLC devices with the structure of ITO/ETL(≈200 nm)/Al, are shown in **Figure 8**. The BPhen:M_2CO_3 blend ETLs were spin coated from FA:H_2O (3:1) solutions with different concentrations of the alkali metal salts to form ≈200-nm thick layers, which were vacuum dried

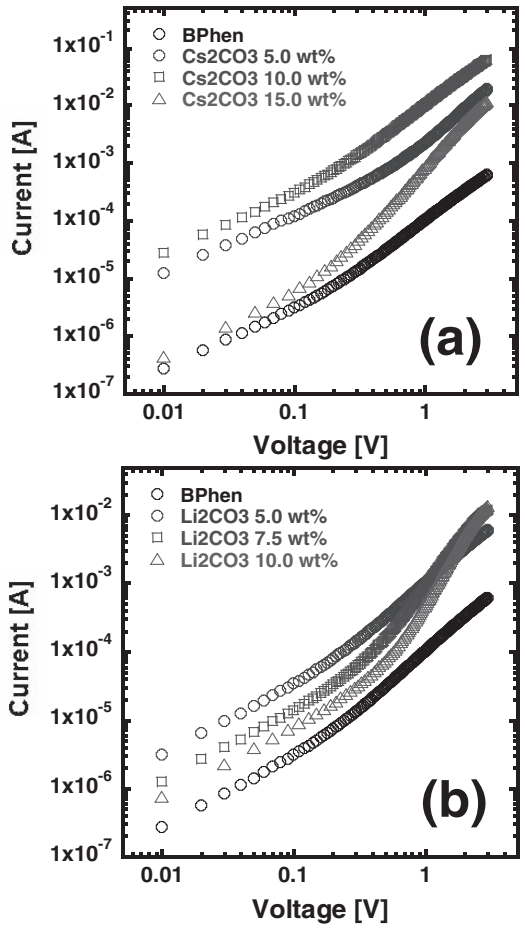

Figure 8. Current-voltage (*I–V*) characteristics of ITO/solution-processed BPhen:alkali metal salt dopant film (≈200 nm)/Al devices in ambient conditions. a) BPhen doped with different concentration of Cs_2CO_3 and b) Li_2CO_3.

overnight at 50 °C followed by Al deposition. The thickness of the BPhen ETLs was measured by a profilometer and also confirmed by AFM measurement. The electron mobility was extracted by fitting the *J–V* curves in the near quadratic region according to the modified Mott-Gurney equation,[59,60]

$$J = \frac{9}{8}\varepsilon\varepsilon_0\mu\frac{V^2}{L^3}\exp\left(0.89\beta\frac{\sqrt{V}}{\sqrt{L}}\right)$$

where J is the current density, ε_0 is the permittivity of free space, ε is the relative permittivity, μ is the zero-field mobility, V is the applied voltage, L is the thickness of active layer, and β is the field-activation factor (**Table 3**). The zero-field electron mobility of the solution-deposited BPhen:M_2CO_3 blend films varied from 4.2×10^{-5} cm^2 V^{-1} s^{-1} without doping, which is consistent with the reported value by SCLC measurement,[55] to 3.7×10^{-3} cm^2 V^{-1} s^{-1} when the doping concentration is 10.0 wt% Cs_2CO_3 (Figure 8a, Table 3). The electron mobility of BPhen with 10.0 wt% Cs_2CO_3 was an order of magnitude higher than that with 5.0 wt% Cs_2CO_3 and two orders of magnitude higher than the non-doped BPhen. Similarly, BPhen doped with 2.5–5.0 wt% Li_2CO_3 had two orders of magnitude higher mobility (1.3×10^{-3} cm^2 V^{-1} s^{-1}) than that of non-doped BPhen.

Table 3. SCLC electron mobility of BPhen ETL at various doping levels.

Dopant	concentration [wt%]	*L* [nm]	β [$cm^{1/2}$ $V^{-1/2}$]	E_{max} [V cm^{-1}]	μ_e ($E = 0$) [cm^2 V^{-1} s^{-1}]
None	0	200	8.7×10^{-6}	1.8×10^5	4.2×10^{-5}
Cs_2CO_3	5.0	200	6.8×10^{-7}	1.8×10^5	5.6×10^{-4}
Cs_2CO_3	10.0	200	8.3×10^{-6}	1.8×10^5	3.7×10^{-3}
Cs_2CO_3	15.0	200	4.9×10^{-5}	1.8×10^5	1.8×10^{-5}
Li_2CO_3	5.0	200	1.3×10^{-5}	1.5×10^5	1.3×10^{-3}
Li_2CO_3	7.5	200	1.1×10^{-5}	1.5×10^5	1.0×10^{-3}
Li_2CO_3	10.0	190	1.5×10^{-5}	1.6×10^5	7.4×10^{-5}

However, further increase of the doping concentration to 15.0 wt% for Cs_2CO_3 and 10.0 wt% for Li_2CO_3, resulted in the electron mobilities dropping to 1.8×10^{-5} and 7.4×10^{-5} cm^2 V^{-1} s^{-1}, respectively. Interestingly, *I–V* curves of the SCLC devices with the highest doping concentrations (15.0 wt% Cs_2CO_3, 7.5 – 10.0 wt% Li_2CO_3) showed steep slopes at high electric field, implying that the current increases faster than V^2. These curvatures indicate the presence of charge trapping sites, which likely originate from the phase separated morphology of the solution-processed BPhen:M_2CO_3 blend ETLs.[61,62]

3. Conclusions

We have showed for the first time that alkali metal salt doped electron-transport layers (ETLs) can be solution-deposited to fabricate high performance, multi-layered, phosphorescent OLEDs. The solution-processing approach is applicable to diverse electron-transport materials and any desirable metal salt. Blue PhOLEDs with solution-deposited Cs_2CO_3-doped TmPyPB ETLs have a luminous efficiency of 37.7 cd A^{-1} with an EQE of 19.0% at a high brightness 1300 cd m^{-2}, which is the highest performance reported to date for all-solution-processed blue PhOLEDs. Studies of the surface morphology and electron transport properties of the alkali metal salt doped electron transport layers showed that doping dramatically enhances the electron mobility and modifies the ETL/cathode interface morphology, enabling efficient electron-injection and transport. The results demonstrated that the properties and nanomorphology of the solution-processed ETLs can be fine-tuned by the concentration of the metal salt (M_2CO_3) and type of metal (M = Cs, Li). The orthogonal solution-processing of multilayered high performance PhOLEDs and metal salt-doped ETLs demonstrated here are also useful for the fabrication of other multi-layered organic electronic devices.

4. Experimental Section

Materials: Poly(*N*-vinyl carbazole) (PVK, average M_w = 1,100,000 g mol^{-1}), 4,7-diphenyl-1,10-phenanthroline (BPhen, 99%, sublimed grade), cesium carbonate (Cs_2CO_3, 99.9% trace metals basis), and lithium carbonate (Li_2CO_3, 99%) were purchased from Sigma-Aldrich Co. 1,3-Bis(2-(4-tert-butylphenyl)-1,3,4-oxadiazo-5-yl)benzene (OXD-7), bis(3,5-difluoro-2-(2-pyridyl)phenyl-(2-carboxypyridyl)iridium(III) (FIrpic), 1,3,5-Tris(m-pyrid-3-yl-phenyl)benzene (TmPyPB), and 1,3-bis(3,5-di(pyridine-3-yl)phenyl)benzene (BmPyPB) were purchased

from Luminescence Technology (LumTec) Co., Taiwan. 1,3,5-tris(4-pyridinquinolin-2-yl)benzene (TPyQB) was synthesized as previously reported.[30] A solution of PEDOT:PSS (poly-(ethylenedioxythiophene):-polystyrenesulfonate, Clevios P VP CH 8000) dispersed in water was purchased from Heraeus GmBH, Germany. All purchased chemicals were used as received without further purification.

Device Fabrication: The phosphorescent emission layer (EML) consisted of a blend of PVK and OXD-7 (PVK:OXD-7 = 60:40, wt/wt) as a host and 10.0 wt% FIrpic as the blue dopant. A solution of PEDOT:PSS was diluted with DI water by 1:1 ratio and filtered before spin-coating to make a 30-nm hole-injection layer onto a pre-cleaned ITO glass. Clevios P VP CH 8000 (PEDOT:PSS) was used to prevent current leakage and suppressing of hole-current.[63] The film was then annealed at 150 °C under vacuum to remove residual water. The 70-nm polymer EML was obtained by spin coating of the PVK:OXD-7:FIrpic blend in chlorobenzene onto the PEDOT:PSS layer and vacuum dried at 100 °C. A small-molecule electron-transport material (ETM, e.g. BPhen) was co-dissolved with alkali metal salt (Cs_2CO_3 or Li_2CO_3) in formic acid:water (FA:H_2O = 3:1) mixture and spun cast onto the EML at a spin speed of 7000 rpm followed by vacuum drying at 50 °C to form an electron-transport layer (ETL). After drying, thermally evaporated Al cathode was deposited onto the ETL. The structure of PhOLEDs with solution-processed ETLs was: ITO/PEDOT:PSS(30 nm)/EML(70 nm)/solution-processed ETM:alkali metal salt (20 nm)/Al (100 nm). The device structure of PhOLEDs with a vacuum-deposited bilayer of BPhen ETL and alkali metal salt was: ITO/PEDOT:PSS(30 nm)/EML(70 nm)/vacuum-deposited BPhen ETL (20 nm)/vacuum-deposited Cs_2CO_3 or Li_2CO_3 (1 nm)/Al. BPhen and alkali metal salt were sequentially vacuum-deposited by thermal evaporation onto EML using Edwards Auto Vacuum 306, followed by a deposition of Al without breaking the vacuum ($<2.0 \times 10^{-6}$ torr).

For the single charge carrier-dominant devices, two types of devices were fabricated. Electron-dominant devices: ITO/polymer host (70 nm)/solution-deposited BPhen:M_2CO_3 ETL (20nm)/Al; and hole-dominant devices: ITO/PEDOT:PSS (30 nm)/polymer host (70 nm)/solution-deposited BPhen: M_2CO_3 ETL (20 nm)/Au. All layers were deposited under exactly the same conditions as the fabrication of PhOLEDs.

Devices for space-charge-limited current (SCLC) measurement were fabricated with ITO/solution-processed BPhen:M_2CO_3 ETL (~200 nm)/Al structure. The organic layer was obtained by the spin-coating of ETM solution onto the substrate followed by deposition of Al electrode.

Characterization: Film thickness was measured by an Alpha-Step 500 profilometer (KLA-Tencor, San Jose, CA) and also confirmed by Atomic Force Microscopy (AFM). Electroluminescence (EL) spectra were obtained using the same spectrofluorimeter described above. Current-voltage (*J*–*V*) characteristics of the PhOLEDs were measured by using a HP4155A semiconductor parameter analyzer (Yokogawa Hewlett-Packard, Tokyo). The luminance (brightness) was simultaneously measured by using a model 370 optometer (UDT Instruments, Baltimore, MD) equipped with a calibrated luminance sensor head (Model 211) and a 5x objective lens. The device external quantum efficiencies (EQEs) were calculated from the forward viewing luminance, current density and EL spectrum assuming a Lambertian distribution using procedures reported previously.[64] All the device fabrication and device characterization steps were carried out under ambient laboratory condition.

Current-voltage characteristics of single charge carrier dominant and SCLC devices were measured using the same semiconductor parameter analyzer as used for PhOLED devices. The measurements were performed under dark and ambient conditions. AFM characterization of surface morphology was done on a Veeco Dimension 3100 Scanning Probe Microscope (SPM) system. The AFM topographical images were directly measured on the same PhOLEDs used for device characterization.

Supporting Information

Supporting Information is available from the Wiley Online Library or from the author.

Acknowledgements

This work was supported by the National Science Foundation (DMR-0805259) and Solvay S. A. Part of this work was conducted at the University of Washington NanoTech User Facility, a member of the NSF National Nanotechnology Infrastructure Network (NNIN).

Received: May 21, 2012
Revised: July 3, 2012
Published online: July 30, 2012

[1] A. P. Kulkarni, C. J. Tonzola, A. Babel, S. A. Jenekhe, *Chem. Mater.* **2004**, *16*, 4556.
[2] F. So, J. Kido, P. Burrows, *MRS Bull.* **2008**, *33*, 663.
[3] A. C. Grimsdale, K. Leok Chan, R. E. Martin, P. G. Jokisz, A. B. Holmes, *Chem. Rev.* **2009**, *109*, 897.
[4] S. Reineke, F. Lindner, G. Schwartz, N. Seidler, K. Walzer, B. Lussem, K. Leo, *Nature* **2009**, *459*, 234.
[5] K. T. Kamtekar, A. P. Monkman, M. R. Bryce, *Adv. Mater.* **2010**, *22*, 572.
[6] Y. Kawamura, S. Yanagida, S. R. Forrest, *J. Appl. Phys.* **2002**, *92*, 87.
[7] C.-H. Yang, Y.-M. Cheng, Y. Chi, C.-J. Hsu, F.-C. Fang, K.-T. Wong, P.-T. Chou, C.-H. Chang, M.-H. Tsai, C.-C. Wu, *Angew. Chem. Int. Ed.* **2007**, *46*, 2418.
[8] T. Earmme, E. Ahmed, S. A. Jenekhe, *J. Phys. Chem. C* **2009**, *113*, 18448.
[9] E. Ahmed, T. Earmme, G. Ren, S. A. Jenekhe, *Chem. Mater.* **2010**, *22*, 5786.
[10] A. Endo, K. Sato, K. Yoshimura, T. Kai, A. Kawada, H. Miyazaki, C. Adachi, *Appl. Phys. Lett.* **2011**, *98*, 083302.
[11] Y. Zhang, C. Zuniga, S.-J. Kim, D. Cai, S. Barlow, S. Salman, V. Coropceanu, J.-L. Brédas, B. Kippelen, S. Marder, *Chem. Mater.* **2011**, *23*, 4002.
[12] a) T.-W. Lee, T. Noh, H.-W. Shin, O. Kwon, J.-J. Park, B.-K. Choi, M.-S. Kim, D. W. Shin, Y.-R. Kim, *Adv. Funct. Mater.* **2009**, *19*, 1625; b) L. Duan, L. Hou, T.-W. Lee, J. Qiao, D. Zhang, G. Dong, L. Wang, Y. Qiu, *J. Mater. Chem.* **2010**, *21*, 6392.
[13] a) B. Ma, B. J. Kim, D. A. Poulsen, S. J. Pastine, J. M. J. Fréchet, *Adv. Funct. Mater.* **2009**, *19*, 1024; b) S. C. Lo, R. N. Bera, R. E. Harding, P. L. Burn, I. D. W. Samuel, *Adv. Funct. Mater.* **2008**, *18*, 3080.
[14] J.-H. Jou, W.-B. Wang, S.-M. Shen, S. Kumar, I. M. Lai, J.-J. Shyue, S. Lengvinaite, R. Zostautiene, J. V. Grazulevicius, S. Grigalevicius, S.-Z. Chen, C.-C. Wu, *J. Mater. Chem.* **2011**, *21*, 9546.
[15] K. S. Yook, J. Y. Lee, *Org. Electron.* **2011**, *12*, 1595.
[16] M. Zhu, T. Ye, X. He, X. Cao, C. Zhong, D. Ma, J. Qin, C. Yang, *J. Mater. Chem.* **2011**, *21*, 9326.
[17] A. C. Arias, J. D. MacKenzie, I. McCulloch, J. Rivnay, A. Salleo, *Chem. Rev.* **2010**, *110*, 3.
[18] F. S. Kim, E. Ahmed, S. Subramaniyan, S. A. Jenekhe, *ACS Appl. Mater. Interfaces* **2010**, *2*, 2974.
[19] S. Sax, N. Rugen-Penkalla, A. Neuhold, S. Schuh, E. Zojer, E. J. W. List, K. Mullen, *Adv. Mater.* **2010**, *22*, 2087.
[20] F. S. Kim, D.-K. Hwang, B. Kippelen, S. A. Jenekhe, *Appl. Phys. Lett.* **2011**, *99*, 173303.
[21] Z.-Y. Liu, S.-R. Tseng, Y.-C. Chao, C.-Y. Chen, H.-F. Meng, S.-F. Horng, Y.-H. Wu, S.-H. Chen, *Synth. Met.* **2011**, *161*, 426.
[22] X. J. Zhang, A. S. Shetty, S. A. Jenekhe, *Macromolecules* **1999**, *32*, 7422.
[23] X. J. Zhang, S. A. Jenekhe, *Macromolecules* **2000**, *33*, 2069.
[24] M. M. Alam, S. A. Jenekhe, *Chem. Mater.* **2002**, *14*, 4775.
[25] C. J. Tonzola, M. M. Alam, W. Kaminsky, S. A. Jenekhe, *J. Am. Chem. Soc.* **2003**, *125*, 13548.

[26] T. W. Kwon, M. M. Alam, S. A. Jenekhe, *Chem. Mater.* **2004**, *16*, 4657.
[27] S. A. Jenekhe, S. J. Yi, *Appl. Phys. Lett.* **2000**, *77*, 2635.
[28] M. M. Alam, S. A. Jenekhe, *Chem. Mater.* **2004**, *16*, 4647.
[29] T. Earmme, E. Ahmed, S. A. Jenekhe, *Adv. Mater.* **2010**, *22*, 4744.
[30] E. Ahmed, T. Earmme, S. A. Jenekhe, *Adv. Funct. Mater.* **2011**, *21*, 3889.
[31] T. Earmme, S. A. Jenekhe, *J. Mater. Chem.* **2012**, *22*, 4660.
[32] A. G. Werner, F. Li, K. Harada, M. Pfeiffer, T. Fritz, K. Leo, *Appl. Phys. Lett.* **2003**, *82*, 4495.
[33] C. K. Chan, W. Zhao, S. Barlow, S. Marder, A. Kahn, *Org. Electron.* **2008**, *9*, 575.
[34] N. Cho, H.-L. Yip, S. K. Hau, K.-S. Chen, T.-W. Kim, J. A. Davies, D. F. Zeigler, A. K. Y. Jen, *J. Mater. Chem.* **2011**, *21*, 6956.
[35] J. Meyer, M. Kröger, S. Hamwi, F. Gnam, T. Riedl, W. Kowalsky, A. Kahn, *Appl. Phys. Lett.* **2010**, *96*, 193302.
[36] K. S. Yook, S. O. Jeon, S.-Y. Min, J. Y. Lee, H.-J. Yang, T. Noh, S.-K. Kang, T.-W. Lee, *Adv. Funct. Mater.* **2010**, *20*, 1797.
[37] K. Walzer, B. Maennig, M. Pfeiffer, K. Leo, *Chem. Rev.* **2007**, *107*, 1233.
[38] D. M. Ivory, G. G. Miller, J. M. Sowa, L. W. Shacklette, R. R. Chance, R. H. Baughman, *J. Chem. Phys.* **1979**, *71*, 1506.
[39] J. Kido, K. Nagai, Y. Okamoto, *IEEE Trans. Electron Devices* **1993**, *40*, 1342.
[40] L. S. Hung, C. W. Tang, M. G. Mason, *Appl. Phys. Lett.* **1997**, *70*, 152.
[41] T. Mori, H. Fujikawa, S. Tokito, Y. Taga, *Appl. Phys. Lett.* **1998**, *73*, 2763.
[42] C. K. Chan, F. Amy, Q. Zhang, S. Barlow, S. Marder, A. Kahn, *Chem. Phys. Lett.* **2006**, *431*, 67.
[43] C. J. Bloom, C. M. Elliott, P. G. Schroeder, C. B. France, B. A. Parkinson, *J. Phys. Chem. B* **2003**, *107*, 2933.
[44] A. G. Werner, F. Li, K. Harada, M. Pfeiffer, T. Fritz, K. Leo, *Appl. Phys. Lett.* **2003**, *82*, 4495.
[45] F. Li, A. Werner, M. Pfeiffer, K. Leo, X. Liu, *J. Phys. Chem. B* **2004**, *108*, 17076.
[46] T. Hasegawa, S. Miura, T. Moriyama, T. Kimura, I. Takaya, Y. Osato, H. Mizutani, *SID Symp. Dig. Tech. Pap.* **2004**, *35*, 154.
[47] C. Wu, C. Lin, Y. Chen, M. Chen, Y. Lu, C. Wu, *Appl. Phys. Lett.* **2006**, *88*, 152104.
[48] Y. Cai, H. X. Wei, J. Li, Q. Y. Bao, X. Zhao, S. T. Lee, Y. Q. Li, J. X. Tang, *Appl. Phys. Lett.* **2011**, *98*, 113304.
[49] Y. Vaynzof, D. Kabra, L. L. Chua, R. H. Friend, *Appl. Phys. Lett.* **2011**, *98*, 113306.
[50] P. Kao, J. Lin, J. Wang, C. Yang, S. Chen, *J. Appl. Phys.* **2011**, *109*, 094505.
[51] M.-H. Chen, Y.-J. Lu, Y.-J. Chang, C.-C. Wu, C.-I. Wu, *Electrochem. Solid-State Lett.* **2010**, *13*, H203.
[52] K. R. Choudhury, J.-H. Yoon, F. So, *Adv. Mater.* **2008**, *20*, 1456.
[53] D. O'Brien, M. A. Baldo, M. E. Thompson, S. R. Forrest, *Appl. Phys. Lett.* **1999**, *74*, 442.
[54] S. Naka, H. Okada, H. Onnagawa, T. Tsutsui, *Appl. Phys. Lett.* **2000**, *76*, 197.
[55] M. A. Khan, W. Xu, H. Khizar ul, Y. Bai, X. Y. Jiang, Z. L. Zhang, W. Q. Zhu, *J. Appl. Phys.* **2008**, *103*, 014509.
[56] S.-J. Su, T. Chiba, T. Takeda, J. Kido, *Adv. Mater.* **2008**, *20*, 2125.
[57] S.-J. Su, Y. Takahashi, T. Chiba, T. Takeda, J. Kido, *Adv. Funct. Mater.* **2009**, *19*, 1260.
[58] S.-J. Su, E. Gonmori, H. Sasabe, J. Kido, *Adv. Mater.* **2008**, *20*, 4189.
[59] N. F. Mott, D. Gurney, *Electronic Processes in Ionic Crystals*, 2nd ed., University Press, Oxford **1948**.
[60] P. N. Murgatroyd, *J. Phys. D: Appl. Phys.* **1970**, *3*, 1488.
[61] M. A. Lampert, *Phys. Rev.* **1956**, *103*, 1648.
[62] S. Jain, *J. Appl. Phys.* **2001**, *89*, 3804.
[63] J. Zou, H. Wu, C.-S. Lam, C. Wang, J. Zhu, C. Zhong, S. Hu, C.-L. Ho, G.-J. Zhou, H. Wu, W. C. H. Choy, J. Peng, Y. Cao, W.-Y. Wong, *Adv. Mater.* **2011**, *23*, 2976.
[64] A. P. Kulkarni, X. X. Kong, S. A. Jenekhe, *J. Phys. Chem. B* **2004**, *108*, 8689.